EasyChair Preprint

№ 5261

A Vaporization Model for Computational Fluid Dynamics Simulations - Application to Film Boiling

Charles Brissot, Rudy Valette and Elie Hachem

March 31, 2021

A VAPORIZATION MODEL FOR COMPUTATIONAL FLUID DYNAMICS SIMULATIONS - APPLICATION TO FILM BOILING

Charles, Brissot[1]
charles.brissot@mines-paristech.fr

Rudy, Valette
rudy.valette@mines-paristech.fr

Elie, Hachem
elie.hachem@mines-paristech.fr

KEY WORDS

Multiphase Flow, Phase Change, Computational Fluid Dynamics, Finite Element Method, Continuous Surface Force.

ABSTRACT

In addition to the challenges of multiphase flow simulation, vaporization phenomena involve important discontinuities of velocity and temperature gradients at the interface. These jumps are crucial to properly tackle the hydrodynamics and thermodynamics of boiling. In this work, we focus on the velocity jump that is computed within a Continuous Surface Force Approach along with a Level Set method. After presenting the model, two benchmarks are presented to validate the efficiency of the method to model the hydrodynamics of film boiling. Comparison is made between the simulations and experimental observations, showing that a laminar approach enable to capture the main features of a vertical film boiling. Then, this method is enriched with a thermal model working in saturated conditions. This complete formulation is used to investigate a 2D film boiling benchmark, validating at the same time the method.

1. INTRODUCTION

Quenching processes involve several complex physical phenomena, among which boiling. Regarding the high temperatures involved, the diversity of sizes and geometries of quenched parts, the comprehension of the whole process is still a challenge. Academics are very active and collaborate with the industry to overcome this, for example with abacus, physical dimensioning and simulations [1–3]. A special interest is taken for boiling, which governs the heat transfer. Drasticity experiments can lead to first arguments on the interaction between the fluid and the solid [4–7]. Physical arguments based on boiling modes advanced by Nukiyama [8] explain general features of all experimental observations. But more precise arguments are needed to predict properly the main aspects of heat exchanges, such as the Leidenfrost temperature, the critical temperature, and the relationships between these parameters and the fluid properties, temperature, convection or the geometry of the quenched part [9–13]. Correlations are a way to describe these parameters without exactly knowing the precise physics beyond [14, 15]. But all these approaches are limited by their lack of universality of correlations or the difficulty to seize all aspects of the physics due to experimental constrains.

This is the reason why numerical simulation has been investigated to bring a deeper comprehension on the physics of quenching and especially on boiling. Pioneer works were done at the beginning of the century to simulate two-phase flows with phase change in 2D [16–19]. A

[1] Corresponding author

majority of the studies on boiling simulations were done with Level Set (LS) or Volume Of Fluid (VOF) methods which are preferred for their simplicity of implementation. Concerning the VOF method, models and correlations are usually employed to tackle the lack of precision regarding the interface position [16, 20–22]. Concerning the LS method, this has the ability to precisely capture the interface, however demanding higher computational costs [23–25].

The latter method is considered in this work, associated with the Continuous Surface Force approach. It has been shown to bring stability to multiphase flow solvers for a simple implementation [26–28] even though it can lack of precision in specific cases [29]. In addition to this, there is a need to develop a proper model to account for the expansion during phase change due to density gaps.

The present works is based on a numerical framework developed by Hachem et al. [30]. The presented method highly builds upon developments made by Khalloufi et al. [25]. To reduce the computational time in prevision of future cases, it is coupled with a remeshing algorithm [31].

In Section 2, the Level Set and the phase change modeling adapted for the framework of the Continuous Surface Force are presented. In Section 3, two benchmarks are presented to validate the presented method. In Section 4, the addition of thermal solver and a benchmark enhancing the performances of the full method are presented.

2. DESCRIPTION OF THE MECHANICAL SOLVER

The fluid motion is governed by the Navier Stokes equations. Fluids are considered incompressible, as the studied velocities are well below the speed of sound. The lagrangian one phase formulation reads:

$$\begin{cases} \vec{\nabla} \cdot \vec{v} = 0 \\ \rho\left(\frac{\partial \vec{v}}{\partial t} + \vec{v} \cdot \vec{\nabla}\vec{v}\right) = -\vec{\nabla}P + \vec{\nabla} \cdot \left(2\,\dot{\varepsilon}(\vec{v})\right) + \rho\vec{g} \end{cases}, \tag{1}$$

where $\vec{v}$ is the velocity field, P is the pressure field, $\dot{\varepsilon}$ is the strain rate tensor, $\vec{g}$ is the gravity field, ρ is the density of the fluid, and η is the dynamic viscosity

For quenching processes, phase change is considered, involving two-phase flows. This entails a need to account for an identification of each phase, effects on the liquid vapor interface, and phase change consideration. In the first place, the rate of surface mass transfer between liquid and vapor is considered to be known, and no energy effects are considered.

2.1 The Level Set formalism

The Level Set formalism is used to identify each phase. The signed distance function $(\underline{x}, I) \mapsto \alpha$ describes the interface I between the two phases:

$$\alpha(\underline{x}, I) = \begin{cases} d(\underline{x}, I) & \text{in the vapor phase} \\ -d(\underline{x}, I) & \text{in the vapor phase} \\ 0 & \text{on the interface} \end{cases}, \tag{2}$$

Practically, the property of distance is lost when the LS is convected, so a reinitialization technique is used. The standard DRT reinitialization is chosen for its simplicity of use [32], and is applied once every a few time iteration. The LS also has the property to have a gradient equal to the normal of the interface. To avoid errors due to the convection, this gradient is normalized and $\vec{n}$ is defined as $\vec{\nabla}\alpha/|\vec{\nabla}\alpha|$.

The associated characteristic function $\alpha \mapsto H_\alpha$ is used as a color function. To avoid numerical instabilities, an interface thickness 2ε is considered, and H_α is smoothed as followed:

$$H_\alpha = \begin{cases} 1 \text{ if } \alpha > \varepsilon \\ \frac{1}{2}\left(1 + \frac{\alpha}{\varepsilon} + \frac{1}{\pi}\sin\left(\frac{\pi\alpha}{\varepsilon}\right)\right) \text{ if } |\alpha| \leq \varepsilon, \\ 0 \text{ if } \alpha < -\varepsilon \end{cases} \quad (3)$$

This allows us to identify both phases and determine the characteristics of a fluid particle regarding the characteristics of the two phases: $x = H_\alpha x_V + (1 - H_\alpha)x_L$. Another useful toll is the smoothed Dirac function $\alpha \mapsto \delta_\alpha$ defined as the derivative of H_α with respect to α:

$$\delta_\alpha = \begin{cases} 0 \text{ if } |\alpha| > \varepsilon \\ \frac{1}{2\varepsilon}\left(1 + \cos\left(\frac{\pi\alpha}{\varepsilon}\right)\right) \text{ if } |\alpha| < \varepsilon' \end{cases} \quad (4)$$

This function enables us to model surface terms as volume terms to be integrated in the Navier-Stokes equations.

2.2 Continuous description of phase change

The vector $\overrightarrow{\dot{m}}$ defines the surface mass change. It is normal to the interface, its norm defines the local intensity of the phase change and its direction indicates condensation of vaporization. The mass change is spread through the interface thanks to the Dirac distribution δ_α [33]. Over an infinitesimal volume dV the local infinitesimal mass transfer rate d$\dot{M}$ is:

$$\mathrm{d}\,\dot{M} = \left(\overrightarrow{\dot{m}} \cdot \vec{\nabla}\alpha\right)\delta_\alpha \mathrm{d}V, \quad (5)$$

$\overrightarrow{\dot{m}}$ is then orthogonal to the interface, assuming that there is no sliding at the interface.

3.1.1 The new mass conservation equation

Such modeling of the mass transfer rate entails the following new source term for the mass conservation equation:

$$\vec{\nabla} \cdot \vec{v} = \left(\frac{1}{\rho_V} - \frac{1}{\rho_L}\right)\left(\overrightarrow{\dot{m}} \cdot \vec{\nabla}\alpha\right)\delta_\alpha, \quad (6)$$

where the subscripts V and L refer to vapor and liquid.

3.1.1 The new Level Set convection equation

The Level Set is convected thanks to the velocity field added with a correction term to account for the mass transfer at the interface and the change of density:

$$\frac{\partial\alpha}{\partial t} + \left(\vec{v} - \frac{\rho}{\rho_V\rho_L}\overrightarrow{\dot{m}}\right) \cdot \vec{\nabla}\alpha = 0, \quad (7)$$

2.3 Governing equations

Following the work of [33], the surface tension can be modeled thanks to a continuous surface force approach:

$$\overrightarrow{f_{ST}} = \sigma\kappa\delta_\alpha\vec{\nabla}\alpha, \quad (8)$$

with σ being the surface tension coefficient and κ the curvature.

Integrating this term to the momentum equation, and considering the other modified equations, the final mathematical system reads:

$$\begin{cases} \vec{\nabla} \cdot \vec{v} = \left(\frac{1}{\rho_V} - \frac{1}{\rho_L}\right)\left(\overrightarrow{\dot{m}} \cdot \vec{\nabla}\alpha\right)\delta_\alpha \\ \rho\left(\frac{\partial\vec{v}}{\partial t} + \vec{v} \cdot \vec{\nabla}\vec{v}\right) = -\vec{\nabla}P + \vec{\nabla} \cdot \left(2\eta\,\dot{\varepsilon}(\vec{v})\right) + \rho\vec{g} + \sigma\kappa\delta_\alpha\vec{\nabla}\alpha, \\ \frac{\partial\alpha}{\partial t} + \left(\vec{v} - \frac{\rho}{\rho_V\rho_L}\overrightarrow{\dot{m}}\right) \cdot \vec{\nabla}\alpha = 0 \end{cases} \quad (9)$$

with ρ and η determined by the following mixing laws:

$$\begin{cases}\rho = H_\alpha \rho_V + (1 - H_\alpha)\rho_L \\ \eta = H_\alpha \eta_V + (1 - H_\alpha)\eta_L\end{cases}, \tag{10}$$

2.4 Numerical implementation

The following equations are solved via a Finite Element Method. The raw weak formulation does not guarantee that the resolution of this formulation with a Galerkin method converges to a proper solution. Important restrictions on the mesh size and the time step are imposed for this formulation to be stable. To avoid such constraints, the Virtual Multi Scale (VMS) is a solution to overcome this difficulty. The VMS method consists in modeling the small scale effects that are not taken into account due to the discrete nature of the formulation. Variations that exist at scales smaller than the mesh size are solved in a dedicated equation. Results of this resolution are injected back into the large scale equation through stabilization terms. The stabilized weak formulation without phase change can be found in [30]. The addition of the mass transfer rate only changes the residual of all equations, ads few source terms to all equations, and modifies the convection velocity of the Level Set convection equation. However the general idea of the VMS stabilization developed in [30] still applies. Further details of this methods and details on the parameters settings are available in [30, 34].

All the numerical methods are achieved using an unstructured mesh through the CIMLib library. When needed, it is refined anisotropically at the interface using the gradient of the hyperbolic tangent of the level set. Each mesh is adapted under the constraint of a fixed, case-dependent number of edges. Most of the time, the adaptation process reduces to the addition of nodes locally in the vicinity of the interface. The near-wake region being accurately captured, the rest of the elements keep the same background size that increases with the distance via three successive refinement steps.

3. APPLICATION OF THE MULTIPHASE FLOW SOLVER

The formulation without phase change have already been tested on several benchmarks [33]. The integration of the phase change terms (that exists only for non zero $\overrightarrow{\dot{m}}$) has however to be tested on a dedicated benchmark.

3.1 A 2D benchmark: constant vaporization of a plane interface

The simplest test that can be done is the convection of a planar interface with a fixed mass transfer: the vapor is stuck at one border of a domain, and the extension due to phase change forces the pushed liquid to escape at the other side of the domain.

The liquid dynamic viscosity η_L is set to $2.80 \times 10^{-4}\ Pa.s$ and the vapor dynamic viscosity η_V is set to $1.20 \times 10^{-4}\ Pa.s$ (the physical values of water and vapor at saturation temperature under atmospheric pressure). The liquid density ρ_L is set to $1000\ kg.m^{-3}$, whereas the value of the vapor density ρ_L is computed from the ratio $r = \rho_L/\rho_v$ that is set to 4 differents values gathered in table 1. $\overrightarrow{\dot{m}}$ is also set to different values so that the interface velocity $\overrightarrow{v_I} = \overrightarrow{\dot{m}}/\rho_V$ is fixed.

Density, ρ (kg/m^3)	500	50	5	0.5
Mass transfer, $\lvert\overrightarrow{\dot{m}}\rvert$ (kg/(m^2.s)	1	0.1	0.01	0.001

Table 1: Density and mass transfer values for every cases

The test is carried out for a square mesh of size $1 * 1\, m^2$, whose mesh size is fixed from $5 \times 10^{-2}\, m$ to $5 \times 10^{-3}\, m$. The time step is fixed accordingly to have a constant CFL number of 0.2, the considered velocity being $\overrightarrow{v_I}$. The interface starts at position $x_0 = -0.3\text{m}$. The mixing length ε is set to $0.05\, m$ for every case. Moreover, no reinitialization is carried out, showing that the correction through $\vec{\nabla}\, \alpha$ is relevant and even sufficient for such simple cases.

Velocity and pressure fields for the configuration $r = 2$ with the finest grid are plotted in Figure 1.

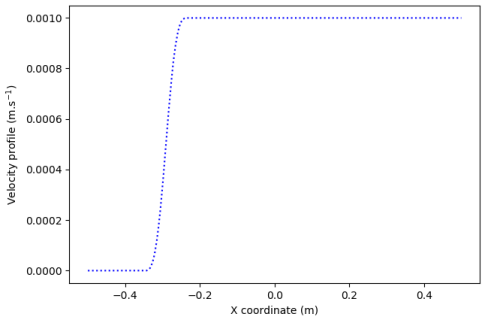

(a): Computed velocity profile

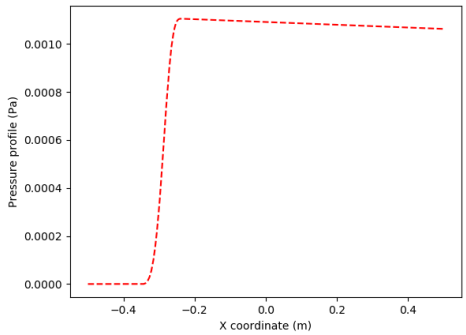

(b): Computed pressure profile

Figure 1: Velocity and pressure fields for the configuration $r = 2$ with the finest grid $h = 5 \times 10^{-3}\, m$. The jumps are smoothened in the framework of the CSF over the total interface length 2ε.

The velocity jump is properly computed and is close to the analytical value. As for the pressure jump, in this configuration no surface tension forces are in play, and normal viscous stresses are negligible. Thus, the pressure jump reads $[\![P]\!] = \overrightarrow{\dot{m}} \cdot [\![\vec{v}]\!] = \left[\!\left[\frac{1}{\rho}\right]\!\right] \overrightarrow{\dot{m}}^2$, whose analytical value $0.001\, Pa$ is coherent with the computed one.

A mesh convergence analysis is carried out. Comparison between the interface position and the analytical solution are plotted in Figure 2, along with the convergence analysis in Figure 3. The convergence order is around 1.66, the model is working well, and the smooth formulation does not bring any numerical error for such conditions.

3.2 A 3D benchmark: vertical film boiling

The formulation is applied on a more complex case: vertical boiling. This is inspired by the experiment of Vijaykumar et al. [11, 12]. They studied the hydrodynamics of the film, and especially the interface perturbations with measuring the wave length, amplitude and rising velocities. This work aims at reproducing the general behavior of the film in the saturated case for $200\, K$ overheating. With velocities of the order of magnitude of $1\, m.s^{-1}$ and a characteristic length of $L = 0.1\, m$ (the solid plate height), this entails a Reynolds of 10^5 in the liquid phase. This would require a huge amount of computational resources as well as a profound stabilization of the scheme. This is due to the perturbations that bring up the liquid at high velocities. This hydrodynamics is quite fine to capture. Thus, as a first approach, we will try to simulate a laminar representation of the flow, with a boosted viscosity in the vapor domain. The film will be more stable, thus diminishing the shear stress at the interface of the water. The objective is here to determine whether it is possible to recover the two main features of the flow, which are the global uprising vapor flow velocity, and the mean film thickness.

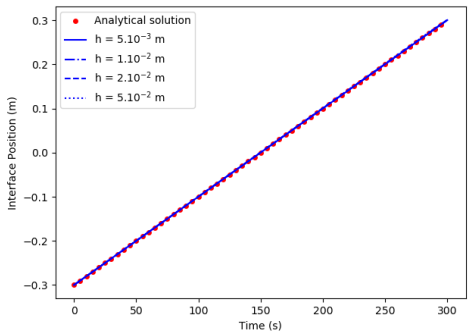

(a): $r = 2$

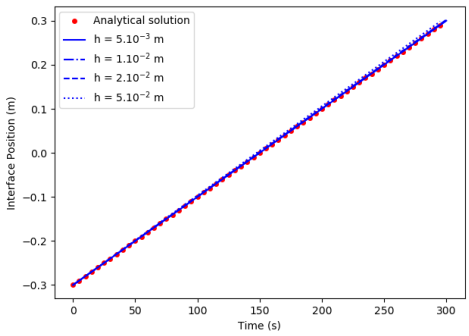

(b): $r = 20$

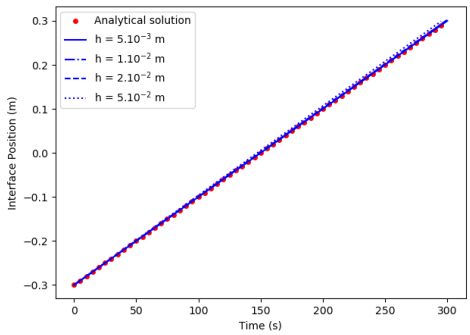

(c): $r = 200$

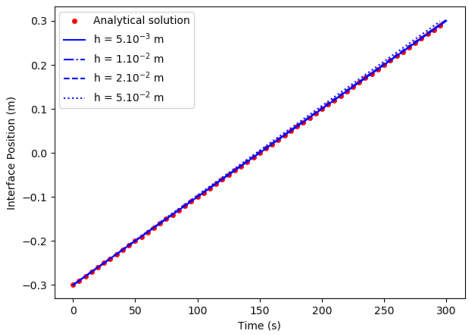

(d): $r = 2000$

Figure 2: Comparison of the position of the convected interfaces for different ratio values and mesh sizes.

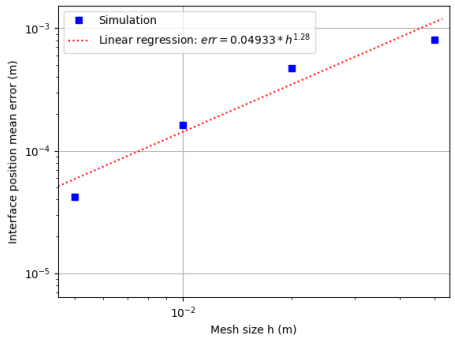

(a): $r = 2$

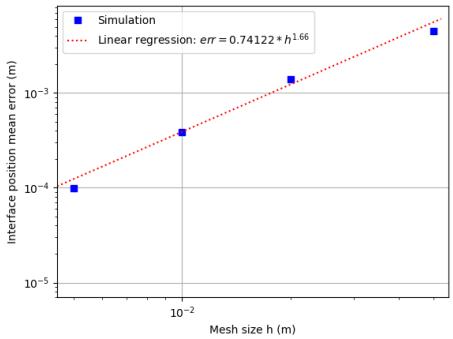

(b): $r = 20$

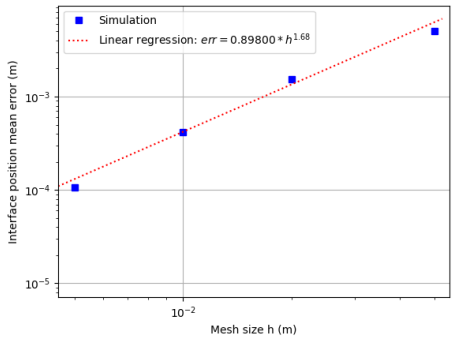

(c): $r = 200$

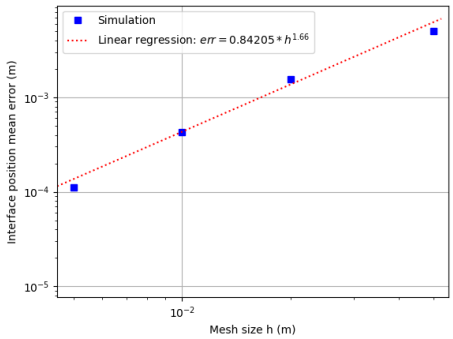

(d): $r = 2000$

Figure 3: Convergence analysis over the interface position mean error for different ratio values.

From the results of Vijaykumar et al [11], the saturated $200\ K$ overheating case shows a vapor wave velocity of $v = 3\ m.s^{-1}$ with a maximum film thickness of e_{max} $10\ mm$. However profiles of waves for saturated cases are not detailed, so an estimation of the mean thickness e_{mean} is needed. The velocity of vapor wave is assumed to be equal to the vapor rising velocity, as every vapor bulk seems to be quite independent of others. In saturated conditions, the heat is almost fully converted in phase change. The rest of the heat is used to warm up the vapor. The latent heat of vaporization of the fluid $\mathcal{L}$ is one order of magnitude higher than $c_{pV}\Delta T$, and most of the vapor does not reach the solid temperature. Thus considering the equality $\vec{q} = \mathcal{L}\overrightarrow{\dot{m}}$ is a reasonable approximation, $\vec{q}$ being the mean heat flux. In [12], the observed heat flux is around $44\ kW.m^{-2}$ leading to a mean value of $0{,}02\ kg.m^{-2}.s^{-1}$ for the mean mass transfer. e_{mean} can be estimated through a balance of mass escaping from the top of the solid thanks to the vapor rising velocity:

$$e_{mean} = \frac{\dot{m}L}{\rho_V v}, \tag{11}$$

This leads to $e_{mean} = 1\ mm$, which is an order of magnitude less than e_{max}: to consider the waves as purely 2D sinusoidal would have been a mistake.

To assess the value of the boosted viscosity η_{eq}, we consider that the shear stress in the vapor film is balancing the hydrostatic pressure. The shear stress gradient scales as $\eta_{eq}v/e^2$, and the pressure gradient as ρg. This leads to an equivalent viscosity: $\eta_{eq} = \rho g e^2/v$. The resulting equivalent viscosity is $3.10^{-3}\ Pa.s$. This value will be used for the viscosity of the vapor. As no thermal aspects are considered, the mass transfer is set according to the desired mean heat flux. However, the local heat flux is not homogeneous, and heat fluxes are more intense where the vapor film is thinner. It is supposed to scale in $1/\mathrm{e}$ (the inverse of the film thickness). Thus, the $\overrightarrow{\dot{m}}$ profile is computed according to a $1/e$ law. Then it is integrated overt the whole surface to recover the effective mean heat flux that is used as a corrective term for the final $\overrightarrow{\dot{m}}$ local value, ensuring the $1/e$ law as well as the mean heat flux value from the experiment.

Properties of the fluid are those of water and liquid, except for the vapor viscosity for which we use the equivalent viscosity determined upward (see table 1).

	Density, ρ (kg/m^3)	Viscosity, η (Pa.s)
Liquid	958	2.80×10^{-4}
Vapor	0.597	3×10^{-3}

Table 2: Density and viscosity values for every phase.

The calculus is set on a domain that is believed to reproduce the test bench of 1992, that is a box of $0{,}17 * 0{,}123 * 0{,}460\ m^3$ with a solid plate of surface $0{,}063 * 0{,}103\ m^2$. The mesh is composed of 500,000 unstructured elements and is refined at the interface up to a mesh size of $5.10^{-4}\ m$. The time step is set to $10^{-3}\ s$.

Visualizations of the interface profile at different time steps are plotted in Figure 4. First, the film waves maintain a 2D aspect due to the laminar modeling of the vapor flow. The wave length is also bigger than the experimental ones, also due to the laminar effect. The mean film thickness is around $2\ mm$, thus a little bigger than the one used for the computation of η_{eq}. However, the order of magnitude is preserved. As for the mean velocity, the estimated value is $0{,}85\ m.s^{-1}$, which is a little lower than the experimental value. However, the order of magnitude is also preserved, confirming the validity of the laminar modeling.

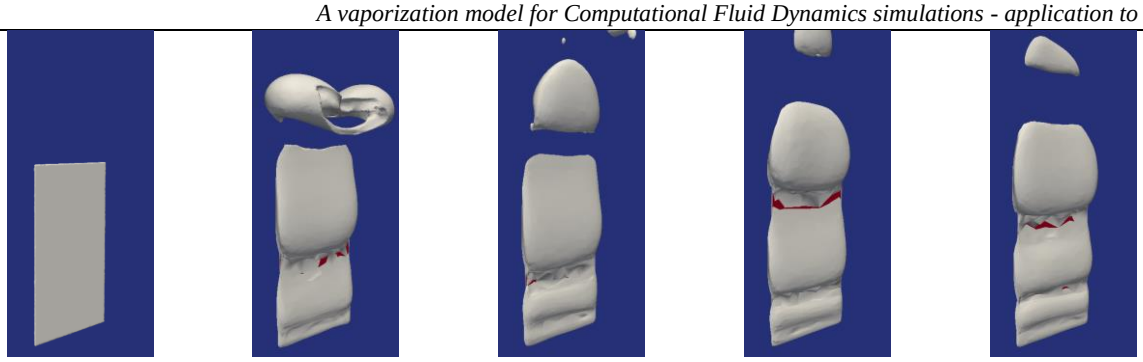

(a): $t = 0s$ **(b)**: $t = 0.25s$ **(c)**: $t = 0.5s$ **(d)**: $t = 0.75s$ **(e)**: $t = 1s$

Figure 4: Interface profiles at different time steps for the 3D vertical film boiling benchmark.

Let us now try to assess the heat flux related to this flow thanks to two simple estimations, through the calculation of the Nusselt number.

$$Nu = \frac{hL_c}{k}, \tag{12}$$

with h the heat transfer coefficient and L_c the characteristic dimension of the problem. It is here taken as the inverse of the critical wave number of the Rayleigh Taylor instabilities:

$$L_c = \sqrt{\frac{\sigma}{(\rho_L - \rho_V)g}}, \tag{13}$$

The first estimation relies on a hypothesis of pure diffusion, meaning that the local heat flux is inversely proportional to the local vapor film thickness e. The heat transfer coefficient $h_{diff} = q_{diff}/\Delta T$ is then only the ratio k_V/e, leading to a Nusselt:

$$Nu_{diff} = \frac{h_{diff}L_c}{k_V} = \frac{L_c}{e}, \tag{14}$$

Another assessment is to add convective effects due to the inner vapor velocity inside the film. A possible estimation of this effect can be set thanks to the Peclet number:

$$Nu_{conv} = (1 + Pe)Nu_{diff}, \tag{15}$$

the Peclet number being defined as:

$$Pe = \frac{\rho c_p e \overline{v_t}}{k}, \tag{16}$$

It enhances the importance of convection over conduction, $\overline{v_t}$ being the mean tangential velocity inside the vapor film. $\overline{v_t}$ can be estimated from the solid surface Σ thanks to the tangential velocity gradient, considering that the tangential vapor flow behaves as a Poiseuille flow:

$$\bar{v} = \frac{e}{6}\left|\frac{\partial \overrightarrow{v_t}}{\partial \vec{n}}\right|_{\underline{x}\in\Sigma}, \tag{17}$$

It is interesting to notice that the vapor mean velocity computed thanks to this estimation leads to a value of $0.65\, m.s^{-1}$, which is close to the first computation, meaning this model of a Poiseuille flow is quite reliable.

The estimation of the Nusselt number compared to the experimental one is plotted on Figure 5. We observed that the experimental value is framed by the two estimations. It is expected that the conductive model underestimates the heat flux, as velocities in play are quite important. As for the conducto-convective model, it overestimates the Nusselt by a factor 4. This is not so surprising as it is based on the assumption that the energy is fully transformed into vapor heating. Thus a volume of vapor flowing on the surface is necessarily a newly created volume. It entails that the vapor should instantly transport the extracted heat far from the solid by vanishing off the solid surface. However here the upper part of the solid is partially covered by vapor that has already absorbed heat from below, meaning that the removed heat is counted more than once. Regarding all these default, the two models still are not so bad as the scale of magnitude is somehow respected. At least it shows once again the relevance of the laminar modeling associated with these estimations.

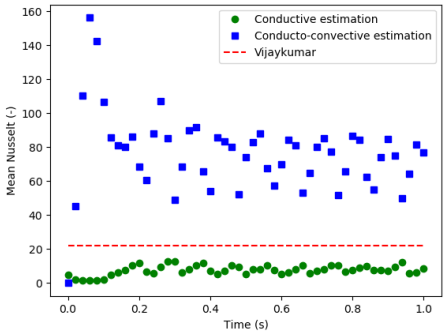

Figure 5: Comparison of the Nusselt over the time between the simulations and the experimental value. The purely conductive and the conducto-convective estimations are plotted in blue.

4. APPLICATION OF THE MULTIPHASE FLOW SOLVER

4.1 Implementation of the temperature convection diffusion equation

We now complete the model with the consideration of energy conservation. Thermal energy variations are assumed to be several orders of magnitude above other forms of energy, and viscous dissipation is considered small in regard to the heat fluxes in play. With this consideration, the energy conservation can be modeled by the convection diffusion equation applied on the temperature field. The source term due to phase change also needs to be integrated. The formalism of the Continuous Surface Force approach allows integrating it in the energy conservation equation as a volume source term:

$$\rho c_p \left(\frac{\partial T}{\partial t} + \vec{v} \cdot \vec{\nabla} T\right) = \vec{\nabla} \cdot \left(k \vec{\nabla} T\right) - \left[\mathcal{L} + \left(c_{pV} - c_{pL}\right)(T - T_{sat})\right]\left(\overrightarrow{\dot{m}} \cdot \vec{\nabla}\alpha\right)\delta_\alpha, \qquad (18)$$

where T is the fluid temperature, k the fluid conductivity and c_p the fluid specific heat capacity.

Now that the energy conservation is solved, the correct computation of $\overrightarrow{\dot{m}}$ can be done. The mass transfer is driven by thermodynamics that motivates the interface to be at thermodynamical equilibrium. Considering the bill of heat flux from both sides of the interface, the remaining available energy is then fully used for phase change. However, the remaining lack of knowledge on transient thermodynamics of phase change generally leads to the need of assumptions to set a coherent model. In this work, we consider that the thermodynamics equilibrium is always maintained, thus interface is set to $T = T_{sat}$, temperature of thermodynamics equilibrium at atmospheric pressure (the effect of the hydrostatic pressure is neglected). The $\overrightarrow{\dot{m}}$ is then computed regarding the available energy, computed by the Heat Flux Jump Computation $\overrightarrow{\dot{m}} = \left[k_V \vec{\nabla} T_{V|\vec{n}} - k_L \vec{\nabla} T_{L|\vec{n}}\right]$ that reduces $\overrightarrow{\dot{m}} = k_V \vec{\nabla} T_{V|\vec{n}}$ in saturated cases. This formulation in addition to the source term in the energy conservation equation theoretically maintains the interface temperature at T_{sat}.

To be consistent regarding the mixing laws of every parameter, a choice is made to consider that H_α is a volume ratio. This entails the mixing law of ρc_p. For the mixing law of k, a harmonic average mean is used following the recommendations of former studies [35, 36] :

$$\begin{cases} \rho c_p = H_\alpha \rho_V c_{pV} + (1 - H_\alpha)\rho_L c_{pL} \\ \frac{1}{k} = \frac{H_\alpha}{k_v} + \frac{1 - H_\alpha}{k_L} \end{cases}, \qquad (19)$$

As it is done for the momentum and mass conservation equations, it is solved via a Finite Element Method along with the VMS method. A complete description of the weak formulation can be found in [37] except for the source term that shall be added.

4.2 Application on the 2D saturated horizontal film boiling benchmark

The 2D saturated film boiling benchmark consists of a horizontal plane solid heated at a constant temperature T_{solid} superior to the saturation temperature T_{sat} of the fluid place above. Thus, the liquid vaporizes. The liquid vapor interface is assumed to remain at Tsat, thus the liquid never touches the solid, and a permanent vapor film is maintained.

The case is solved in 2D, and a comparison is done between the obtained mean heat flux and experimental data [38, 39] through the calculation of the Nusselt Number. L_c is again taken as the characteristic dimension of the problem. It is here taken as the inverse of the critical wave number of the Rayleigh-Taylor instabilities. The interface is initialized by a perturbation whose wavelength λ_{max} is the most unstable wavelength of the RT instabilities:

$$\lambda_{max} = 2\pi\sqrt{3}L_c \,, \tag{20}$$

The fluids properties are as follow:

	Density, ρ (kg/m^3)	Viscosity, η (Pa.s)	Specific heat capacity, c_p (J./(kg.K))	Conductivity, k (W/m.K)	Specific latent heat of vaporization, $\mathcal{L}$ (J/kg)
Liquid	200	0.1	400	40	10000
Vapor	5	0.005	200	1	

Table 3: Physical values of every phases used for the simulation.

The case is solved on a $0.08 * 0.4\, m^2$ domain, and runs on a 50,000 elements mesh whose mesh size is refined at the interface up to $10^{-4}\, m$. Two solid temperatures are considered: 5 K and 10 K above saturation temperature.

The phases distribution profiles at different time steps for an overheating of 5 K are described in Figure 6. The typical mushroom shape observed by [33, 40, 41] is well reproduced here.

(a): $t = 0s$ **(b)**: $t = 0.25s$ **(c)**: $t = 0.5s$ **(d)**: $t = 0.75s$ **(e)**: $t = 1s$

Figure 6: Phases distribution profiles at different time steps for the 2D film boiling benchmark for an overheating of 5 K. The configuration of the simulation leads to a mushroom shaped bubble with a stable tail.

The computed Nusselt are plotted in Figure 7 and compared with the correlations of [38] and [39]. Results are close to those obtained by [41], that is a Nusselt that tends closely to the correlation of Klimenko. This shows the relevancy of our model for such boiling modes.

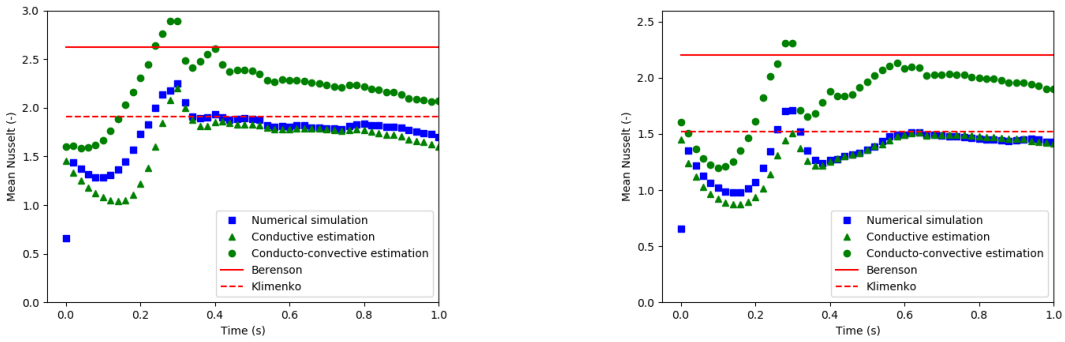

(a) $\Delta T = 5K$ **(b)**: $\Delta T = 10K$

Figure 7: Comparison of the Nusselt over the time between the simulations with the correlations of [38] and [39] for two overheating 5K and 10K. The purely diffusive and the convector-diffusive estimations are plotted in blue.

Let us compute the two estimations of Nusselt on this case and compare them with the simulation by plotting it on the same Figure 7, on blue. What can be deduced is that the major part of heat fluxes is conduction effects: the convection contribution is here overestimated by more than a factor 4, meaning that the associated modeling is only relevant for sufficiently high Peclet number.

5. CONCLUSIONS

First, a mechanical solver to compute velocity jumps across an interface has been presented, and tested on two different benchmarks. It has then been completed along with a thermal solver to account for the energy aspects that drive the mass transfer. The validity of both the mechanical and thermomecanics formulation has been verified on 2D and 3D benchmarks. What can be concluded is that for vaporization modes that are laminar enough, the model runs smoothly, and results are coherent with analytical and experimental observations. Laminar approximations can give meaningful insights on the hydrodynamics of film boiling. What is missing is however to account for temperatures inside the liquid phase, that might cool down the interface and reduce the energy available for vaporization. This complete heat flux jump computation is quite tricky and needs a dedicated work. Then, a more robust method needs to be developed to tackle more turbulent vaporization flows. Furthermore, wetting is still not implemented here, and only film boiling modes can be simulated.

ACKNOWLEDGEMENTS

The authors are thanksfull to the industrials of the Infinity chair for the funding of these works.

REFERENCES AND CITATIONS

[1] Barberis, P. (2018). Traitements thermiques des alliages de zirconium et de hafnium. *Techniques de l'Ingénieur, M1345 V1*, 1‑25.

[2] Bristiel, P., & Niane, N. T. (2013). Simulation numérique des traitements thermochimiques : applications industrielles. *Techniques de l'Ingénieur*, IN209 V1, 1-24.

[3] Murry, G. (2000). Traitements thermiques dans la masse des aciers. Partie 1. *Techniques de l'Ingénieur, M1126 V1*, 1‑25.

[4] Ebrahim, S. A., Chang, S., Cheung, F.-B., & Bajorek, S. M. (2018). Parametric investigation of film boiling heat transfer on the quenching of vertical rods in water pool. *Applied Thermal Engineering, 140*, 139‑146.

[5] Ramesh, G., & Narayan Prabhu, K. (2014). Assessment of axial and radial heat transfer during immersion quenching of Inconel 600 probe. *Experimental Thermal and Fluid Science, 54*, 158‑170.

[6] Buczek, A., & Telejko, T. (2013). Investigation of heat transfer coefficient during quenching in various cooling agents. *International Journal of Heat and Fluid Flow, 44*, 358‑364.

[7] Vergara-Hernández, H. J., & Hernández-Morales, B. (2009). A novel probe design to study wetting front kinematics during forced convective quenching. *Experimental Thermal and Fluid Science, 33*(5), 797‑807.

[8] Nukiyama, S. (1934). The maximum and minimum values of the heat Q from metal to boilng water under atmospheir pressure. *Journal of Japan Society of Mechanical Engineering, 37*, 367‑374.

[9] Ramilison, J. M., & Lienhard, J. H. (1987). Transition Boiling Heat Transfer and the Film Transition Regime. *Journal of Heat Transfer, 109*(3), 746‑752.

[10] Feng, Q., & Johannsen, K. (1991). Experimental results of maximum transition boiling temperature during upflow in a circular tube at medium pressure. *Experimental Thermal and Fluid Science, 4*(1), 90‑102.

[11] Vijaykumar, R., & Dhir, V. K. (1992). An Experimental Study of Subcooled Film Boiling on a Vertical Surface—Hydrodynamic Aspects. *Journal of Heat Transfer, 114*(1), 161.

[12] Vijaykumar, R., & Dhir, V. K. (1992). An Experimental Study of Subcooled Film Boiling on a Vertical Surface—Thermal Aspects. *Journal of Heat Transfer, 114*(1), 169.

[13] Ikkene, R., Koudil, Z., & Mouzali, M. (2008). Pouvoir de refroidissement des solutions de trempe à base de polymères hydrosolubles. *Comptes Rendus Chimie, 11*(3), 297‑306.

[14] Chen, J. C. (1966). Correlation for Boiling Heat Transfer to Saturated Fluids in Convective Flow. *Industrial & Engineering Chemistry Process Design and Development, 5*(3), 322‑329.

[15] Cooper, M. G. (1984). Saturation Nucleate Pool Boiling - A Simple Correlation. In *First U.K. National Conference on Heat Transfer* (p. 785‑793). Elsevier.

[16] Lee, W. H. (1980). A Pressure Iteration Scheme for Two-Phase Flow Modeling. *Mathematical Modeling*, 61‑82.

[17] Son, G., & Dhir, V. K. (1998). Numerical Simulation of Film Boiling Near Critical Pressures With a Level Set Method. *Journal of Heat Transfer, 120*(1), 183‑192.

[18] Juric, D. (1998). Computations of Boiling Flows. *International Journal of Multiphase Flow*, 24.

[19] Welch, S. W. J., & Wilson, J. (2000). A Volume of Fluid Based Method for Fluid Flows with Phase Change. *Journal of Computational Physics*, *160*(2), 662‑682.

[20] Bo, T. (2004). CFD Homogeneous Mixing Flow Modelling to Simulate Subcooled Nucleate Boiling Flow. *SAE Technical Paper Series*.

[21] Rattner, A. S., & Garimella, S. (2014). Simple Mechanistically Consistent Formulation for Volume-of-Fluid Based Computations of Condensing Flows. *Journal of Heat Transfer*, *136*(7).

[22] Ramezanzadeh, H., Ramiar, A., & Yousefifard, M. (2017). Numerical investigation into coolant liquid velocity effect on forced convection quenching process. *Applied Thermal Engineering*, *122*, 253‑267.

[23] Tanguy, S., Ménard, T., & Berlemont, A. (2007). A Level Set Method for vaporizing two-phase flows. *Journal of Computational Physics*, *221*(2), 837‑853.

[24] Denis, R. (2014). Modélisation et simulation de l'effet Leidenfrost dans les micro-gouttes. Université de Grenoble.

[25] Khalloufi, M., Valette, R., & Hachem, E. (2020). Adaptive Eulerian framework for boiling and evaporation. *Journal of Computational Physics*, *401*, 109030.

[26] Unverdi, S. O., & Tryggvason, G. (1992). A Front-Tracking Method for Viscous, Incompressible, Multi-fluid Flows. *Journal of Computational Physics*, 25‑37.

[27] Sussman, M., Smereka, P., & Osher, S. (1994). A Level Set Approach for Computing Solutions to Incompressible Two-Phase Flows. *Journal of Computational Physics*, *114*, 146‑159.

[28] Osher, S., & Fedkiw, R. (2004). *Level set methods and dynamic implicit surfaces* (Vol. 153). Springer.

[29] Tanguy, S., Sagan, M., Lalanne, B., Couderc, F., & Colin, C. (2014). Benchmarks and numerical methods for the simulation of boiling flows. *Journal of Computational Physics*, *264*, 1‑22.

[30] Hachem, E., Khalloufi, M., Bruchon, J., Valette, R., & Mesri, Y. (2016). Unified adaptive Variational MultiScale method for two phase compressible–incompressible flows. *Computer Methods in Applied Mechanics and Engineering*, *308*, 238‑255.

[31] Hachem, E., Feghali, S., Codina, R., & Coupez, T. (2013). Immersed stress method for fluid-structure interaction using anisotropic mesh adaptation: a monolithic approach to fluid-structure interaction. *International Journal for Numerical Methods in Engineering*, *94*(9), 805‑825.

[32] Florez, S., Shakoor, M., Toulorge, T., & Bernacki, M. (2020). A new finite element strategy to simulate microstructural evolutions. *Computational Materials Science*, *172*, 109335.

[33] Khalloufi, M. (2018). Multiphase flows with phase change and boiling in quenching processes. Mines ParisTech.

[34] François, G. (2011). Éléments finis stabilisés pour le remplissage en fonderie à haut Reynolds. Mines ParisTech.

[35] Patankar, S. V. (1980). *Numerical heat transfer and fluid flow*. New York: Hemisphere Publ. Co.

[36] Hachem, E. (2009). *Stabilized finite element method for heat transfer and turbulent flows inside industrial furnaces* (PhD Thesis).

[37] Hachem, E., Rivaux, B., Kloczko, T., Digonnet, H., & Coupez, T. (2010). Stabilized finite element method for incompressible flows with high Reynolds number. *Journal of Computational Physics*, *229*(23), 8643‑8665.

[38] Berenson, P. J. (1960). *Transition Boiling Heat Transfer from a Horizontal Surface* (Technical Report No. 17). The National Science Foundation.

[39] Klimenko, V. V. (1981). Film boiling on a horizontal plate — new correlation. *International Journal of Heat and Mass Transfer*, *24*(1), 69‑79.

[40] Esmaeeli, A., & Tryggvason, G. (2004). Computations of film boiling. Part I: numerical method. *International Journal of Heat and Mass Transfer*, *47*(25), 5451‑5461.

[41] Akhtar, M. W., & Kleis, S. J. (2013). Boiling flow simulations on adaptive octree grids. *International Journal of Multiphase Flow*, *53*, 88‑99.